Journal of Research in Science and Engineering (JRSE)
ISSN: 1656-1996 Volume-7, Issue-6, June 2025
DOI: 10.53469/jrse.2025.07(06).11

Optimization of Structural Parameters of Air Pump Spring based on Machine Learning

Pengxiao Wang[1], Xuecheng Ping[2,*], Qianqian Liu[3]

[1,2,3]College of Mechanical Engineering, Tianjin University of Science and Technology, Tianjin 300222, China
[1,2,3]Tianjin Key Laboratory of Integrated Design and On-line Monitoring for Light Industry & Food Machinery and Equipment, Tianjin 300222, China
Correspondence Author

Abstract: ***Spring leaves usually need to bear huge load and impact, thus wear, fracture, fatigue and other forms of failure easily take place. In this paper, the fatigue behavior of the air pump spring is numerically analyzed by finite element simulation technology. Based on the finite element result data set and the improved particle swarm BP neural network, the mapping relationship between spring structural parameters and fatigue damage is established. With the combination of neural network and genetic algorithm, a spring structure optimization method is proposed, and on this basis, the structural parameters of air pump springs are optimized by multi-objective, to improve its fatigue resistance. This study provides a reference for the health management of air pump spring, a new idea for its structure optimization.***

Keywords: Piston booster air pump, Spring leaf, Fatigue strength, Structure optimization.

1. Introduction

Air pumps play an irreplaceable role in biomedical, aerospace, and oil and gas [1]. Piston booster air pumps suck in and compress gas through a piston that reciprocating in a cylinder with a wide variety of valve designs. As shown in Figure 1, the ventilation valve port of a booster air pump is composed of a spring sheet and an intermediate block, and the outlet is equipped with a limiting block and is fixed by rivets. The air pump drives the piston to move through the shaft drive the crank, and the spring plate opens or resets under the action of air pressure. The springs reciprocate frequently during operation to ensure air tightness and normal operation of the system. The spring disc needs to have high flexibility to allow the fluid to pass through, and it must be rigid enough to close the valve port in time, so it must have the comprehensive performance of the valve disc and the spring.

However, long-term mechanical loads and repeated deformations can easily lead to fatigue fracture of spring blades [2]. In practical engineering problems, people pay more attention to the key factors that affect fatigue. To this end, He et al. proposed a cumulative fatigue damage saturation model [3], Naderi et al. [4] proposed a method for predicting the fatigue life of metals based on cyclic plastic strain energy. Lin [5] proposed a model that combined Miner-Palmgren and S-N curves and took into account the loading situation. These methods rely on empirical formulas and simplified assumptions, and fail to account for the interaction of multiple factors in practical engineering. The finite element method has become an important means to predict stress changes. Xu et al. [6] used the finite element model to study the effects of preload and friction coefficient on the stress of the contact surface, Xu Zhipeng et al. [7] analyzed the fatigue life of the connecting rod based on the finite element method, Zhang et al. [8] used the finite element method to analyze and simulate the natural loosening of bolts under wear conditions. Afolabi et al. [9] studied the fatigue life parameters and plastic deformation of the machine shaft through finite element analysis. The finite element method is widely used in dealing with complex engineering problems, but it still faces challenges such as large computational amount and long calculation cycle.

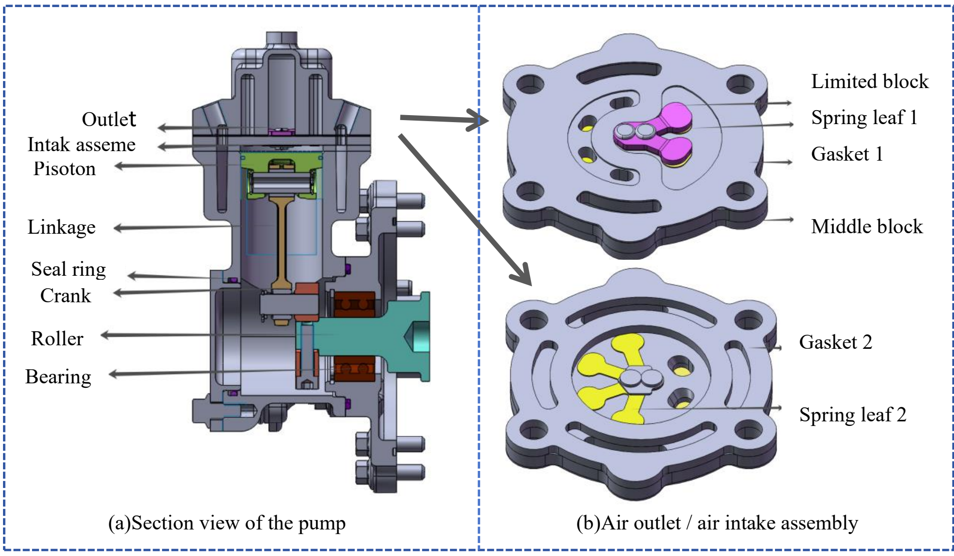

Figure 1: Schematic diagram of piston booster pump structure

As a data-driven science, machine learning can effectively establish nonlinear models by virtue of its big data foundation and the advantages of no complex theoretical analysis, and can be widely used in problems with complex mapping relationships. Ankit et al. [10] discussed the application of deep learning to different material data, and analyzed its progress and application potential in various fields. Han et al. [11] used deep learning to predict the cracking location of fretting fatigue cracks, Srinivasan et al. [12] assessed the low-cycle fatigue life of 316L stainless steel using a neural network; Peng Chao et al. [13] established a BP artificial neural network that reflects the mapping relationship between the structural parameters of the release trough and the stress-strain. Peng [14] used a three-layer LMBP neural network to predict the fatigue life of coiled tubing. Zhang et al. [15] used deep learning models to predict creep, fatigue, and creep fatigue life of materials. Brito et al. [16] proposed a hybrid model combining artificial neural networks and non-local multiaxial fatigue analysis to predict fretting fatigue life. In summary, artificial neural networks can accurately map the nonlinear relationship between data and effectively improve the prediction accuracy, and machine learning has been more widely used in the study of fatigue problems.

Regarding the optimal design of the influencing parameters of mechanical design, Xin [17] used BP neural network as the objective function and gamultiobj function to carry out the lightweight optimization design of automobile bracket. Fares et al. [18] carried out multi-objective optimization based on the Lipno-Belman theory. Peng et al. [19] used genetic algorithm to consider the optimization objectives and optimization conditions, and obtained the optimal palletizing sequence and material distribution. Song et al. [20] expressed the unknown relationship between the design variable and the objective function based on finite element analysis and response surface method, combined with the NSGA-II genetic algorithm, to optimize the structural parameters. Yas et al. [21] used genetic algorithm to optimize the layer arrangement under load. While these studies focus on optimizing the design, this study uses the data results obtained by the neural network as input variables, thus improving the design process.

The main purpose of this study is to construct a finite element simulation model of air pump springs, and on this basis, an optimization method combining neural network and genetic algorithm is proposed to realize the optimal design of spring structural parameters and effectively improve the fatigue resistance of springs.

2. Physical Model

2.1 Mathematical Model of the Fatigue Strength of the Spring Sheet

Prediction and evaluation of fatigue life often involves several factors, including the nature of the material, loading conditions, environmental factors, and the geometry of the design. In complex engineering systems, the influencing factors of fatigue life are more complex. In the past, the critical plane method has been widely used in predicting the initiation life of multiaxial fatigue cracks, and the commonly used criteria in the critical plane method include the stress-based Findley parameter (FP), the strain-based Fatemi-Social parameter (FS), and the strain energy density-based Smith-Watson-Topper (SWT) parameters. Among them, the SWT parameter was proposed by Smith et al., which can effectively solve the problem of multi-axis fatigue. The life is greatly affected by the load characteristics, such as the magnitude and fluctuation of the load, and the SWT damage parameters are determined by the maximum normal stress $\sigma_{n,max}$ and the normal strain amplitude $\Delta\varepsilon_{n,a}$ in a load cycle. It is expressed as:

$$SWT = \sigma_{n,\ max}\varepsilon_{n,\ a} = \frac{(\delta_f)^2}{E}\left(2N_f\right)^{2b} + \sigma_f^{'}\varepsilon_f^{'}\left(2N_f\right)^{b+c} \quad (1)$$

where E is the elastic modulus of the material, N_f is the fatigue life, σ_f' is the fatigue strength coefficient, b is the fatigue strength index, ε_f' is the fatigue toughness coefficient, and c is the fatigue toughness index.

2.2 Data Acquisition

In the field of machine learning, large and diverse data is the key to model training and optimization. Therefore, the numerical simulation method is used to generate the dataset, which can provide rich samples for the model, so as to improve the accuracy and generalization ability of the model. By changing different parameter levels for numerical simulation, the distribution results of SWT damage parameters and displacements under each parameter combination can be obtained.

Three design variables were selected, and the design parameters of the spring sheet were thickness D, width X, and fillet R, as shown in Figure 2(a). The size level of the three design parameters is based on the original size of the spring sheet, and a reasonable range containing the original size is selected. D selected 6 size levels, X and R selected 4 parameter levels, and the spring blades with different parameter combinations were modeled, and Abaqus was used for finite element analysis. For the convergence of the mesh, as shown in Figure 2(b), when the mesh size is 0.05mm, the analysis results show good stability and meet the simulation accuracy requirements. Therefore, this size was selected to mesh the model, and 1236839 C3D8 element meshes were established. Ninety-six finite element simulations were carried out for the combination of geometric parameters of different sizes of springs, and the distribution of stress and SWT damage parameters of springs, as well as their maximum displacement U, were further obtained through finite element simulations. The *SWT* is output by Uvarm, a custom subroutine in Abaqus. The specific process is as follows, firstly, the stress-strain data of each node obtained by simulation is extracted, secondly, the different angle planes at each position are obtained as alternative planes through the coordinate conversion equation, and then the maximum normal stress and normal strain amplitude on each plane are extracted to obtain the corresponding SWT values on each alternate plane, and the plane where the maximum SWT is located in the alternative plane at each position is selected as the critical plane, and the distribution of the maximum SWT value is further obtained.

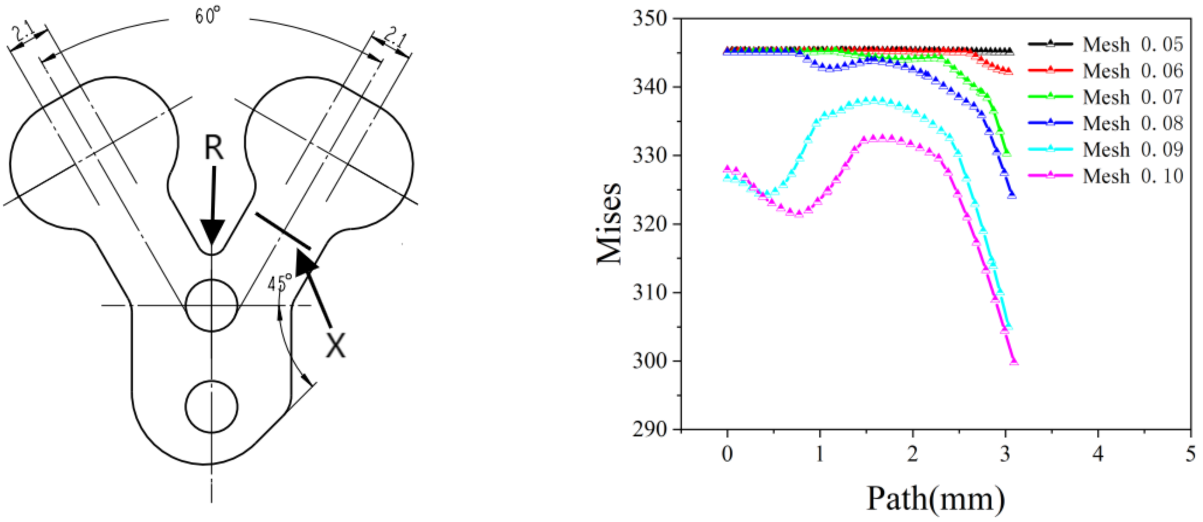

(a) Spring parameters (b) Grid convergence

Figure 2: Spring structure and mesh Convergence

3. PSO-BP Surrogate Model

3.1 PSO-BP Agent Model Construction

BPNN is a multi-layer feedforward neural network that uses a backpropagation algorithm to optimize the weights and biases of the network to minimize the prediction error. Considering that the BP algorithm is easy to fall into the local optimal solution, the global search ability of the PSO algorithm is combined with the local search ability of the BP algorithm, and the improved particle swarm optimization algorithm (PSO) is used to search for the optimal initial weight and threshold, which can effectively avoid the problem of local optimum. As a result, the initial weight jumps out of the local extremum, which helps to accelerate the convergence process and enhance the accuracy and generalization ability of BPNN.

In the standard PSO algorithm, the inertia weight is a key influencing parameter in the tunable parameters of the algorithm. The nonlinear inertia weights used in this paper help to balance the global and local search capabilities, and the equation is as follows:

$$w^t = w\left(wmin_{max}\cdot\left(\frac{t}{t_{max}}()^2\right)\right)_{max} \tag{2}$$

where w_{max} and w_{min} are the maximum and minimum inertia weights, which are set to 0.9 and 0.4.

In addition, the learning factor determines the optimal trajectory of the particle to a certain extent. So improvements were made to the evolution of the asynchronous learning factors used:

$$c_1^t = c_{1s} + (c_{1e} - c_{1s})\cdot\frac{t}{t_{max1s1e}} \tag{3}$$

$$c_2^t = c_{2s} + (c_{2e} - c_{2s})\cdot\frac{t}{t_{max2s2e}} \tag{4}$$

where c_{1s} and c_{1e} are the start and end values of c_1, respectively. The similarity c_{2s} and c_{2e} represent the start and end values of c_2, respectively. Therefore, in the early stage of iteration, $c_1 > c_2$, enhances the global search capability and prevents premature convergence to the suboptimal solution. In the later stage of iteration, $c_1 > c_2$, which is conducive to strengthening the local search and accelerating the convergence to the global optimal solution.

Therefore, PSO-BPNN was used to deal with the mapping relationship between the influencing factors and the response, and the sample set obtained by numerical simulation was divided into a training set and a test set, as shown in Figure 3, the input layer included three neurons, the thickness of the spring blade (*D*), the transition arc radius (*R*) and the bifurcation width (*X*), and then *SWT* and *U* were used as the output layers to train two neural networks.

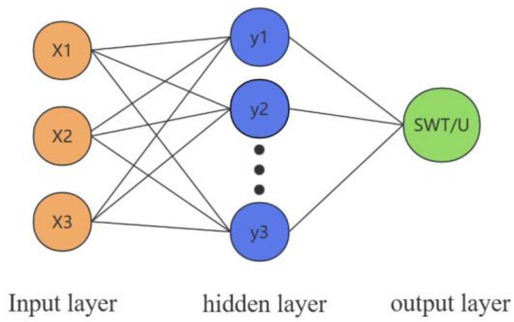

Figure 3: Neural network structure

3.2 PSO-BP Neural Network Analysis

The ability of the neural network trained based on the PSO-BPNN model to predict *SWT* and *U* is evaluated by scatter plots, and Fig. 4 shows that the predicted values of the PSO-BP neural network are in good agreement with the finite element calculation results.

For the neural network with *SWT* as output, the R^2 values of the training set and the test set were 0.99795 and 0.9945, and the MAE were 0.0068713 and 0.01218; respectively, and for the neural network with *U* as output, the R^2 values were 0.99912 and 0.99899, and the MAE were 0.0018107 and 0.0021919, respectively. Moreover, the prediction errors of the two neural networks for *SWT* and *U* are within the range of 5% (black dotted line), as shown in Figure 4(c)-(f). The above results show that the prediction results are in good agreement with the calculation results of the physical model, which proves the prediction ability of the model.

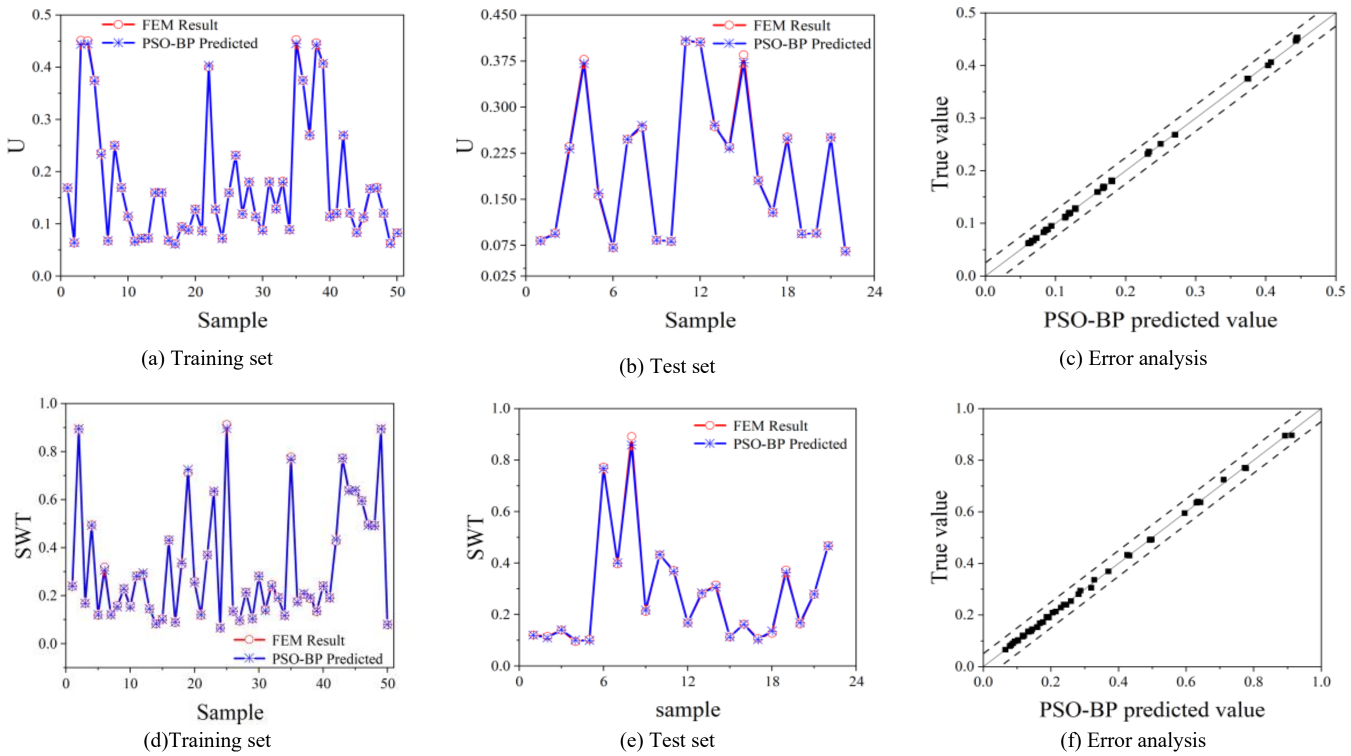

Figure 4: Neural network prediction result

Table 1: PSO-BPNN prediction output 1 result error

K_i	1	2	3	4	5	6
Training R^2	0.97969	0.99087	0.99214	0.99429	0.99278	0.98247
Test R^2	0.97266	0.92076	0.98303	0.95652	0.94697	0.98056
Training MAE	0.025841	0.018162	0.012479	0.010113	0.013219	0.014726
Test MAE	0.022522	0.013862	0.020949	0.038754	0.032735	0.01464

Table 2: PSO-BPNN prediction output 2 result error

K_i	1	2	3	4	5	6
Training R^2	0.99108	0.99752	0.98054	0.98058	0.94708	0.97369
Test R^2	0.95387	0.94765	0.98633	0.97025	0.94589	0.98152
Training MAE	0.011488	0.0047275	0.02517	0.023661	0.012016	0.02506
Test MAE	0.039426	0.013583	0.02924	0.028541	0.013319	0.02522

Then, K-fold cross-validation (K takes 5) was used to evaluate the accuracy of the model and verify the generalization performance. The dataset is divided into 5 parts, one of which is used as the test set, and the remaining 4 are used as the training set for multiple training and verification, which can verify the reliability of the method under limited data, and has a good effect on evaluating the generalization ability of the model and selecting the best combination of hyperparameters. Finally, the Mean Absolute Error (MAE) was compared to discuss the cross-validation results, and the influence of different data partitions on the prediction accuracy of the neural network model was analyzed.

Table 1 and Table 2 show the K-fold cross-validation prediction results, and it can be seen that the accuracy of the prediction results can be maintained at a high level under different data partitioning methods, and the performance parameters remain stable, which shows that the data partitioning has little impact on the prediction results of the neural network, which further reflects that the prediction model has good prediction accuracy and generalization ability.

4. Optimization Method

4.1 Parametric Analysis

Orthogonal experiments (DOE) were used to analyze the sensitivity of the main design factors. Four different values of the three factors were selected as DOE levels, as shown in Table 3. *SWT* and maximum displacement *U* were selected as the responses to DOE. 16 sets of experimental data were generated using array $L_{16}(4^3)$. The range analysis method was used to analyze the sensitivity of each influencing factor, and the range contribution of each input parameter to the output was calculated. Firstly, the amplitude of *SWT* and *U* at different levels of each factor is given, as shown in Table 4.

Table 3: Orthogonal experimental level

	D/mm	*R*/mm	*X*/mm
1	0.3	0.7	3.6
2	0.35	1	3.9
3	0.4	1.5	4.2
4	0.45	2	4.5

Table 4: The change range of response at different levels

	D/mm	*R*/mm	*X*/mm
n_{1i}	2.762624	1.718842	1.922019
n_{2i}	1.576569	1.65128	1.658529
n_{3i}	1.036765	1.473735	1.38399
n_{4i}	0.721459	1.25356	1.132879
m_{1i}	1.452915	0.97056	1.029403
m_{2i}	0.972922	0.938112	0.943906
m_{3i}	0.658828	0.908835	0.889591
m_{4i}	0.466975	0.869241	0.823848

Note: n_{ji} is the *SWT* change amplitude of factor i at different levels, and m_{ji} is the *U* change amplitude of factor i at different levels.

By analyzing and identifying the magnitude of the range difference of different influencing factors, the influence degree of different design parameters on the working performance of the spring sheet can be obtained, and then the sensitivity of different factors can be obtained, as shown in Figure 5:

The order of the test factors on the *SWT* of spring blades was as follows: factor 1 (D) > factor 3 (X) > factor 2 (R).

The order of the test factors influencing the maximum *U* of the spring disc is as follows: factor 1 (D) > factor 3 (X) > factor 2 (R).

As can be seen from Figure 6, the change trend of the maximum *SWT* and *U* is consistent with the change of D and R, and both decrease with the increase of the factor level, among them, the *SWT* reaches the maximum value at the radius of the circular line of about 1.4mm, but the displacement *U* should not be too small because the spring blade needs to ensure that the air can pass smoothly to meet the requirements of work efficiency. As *X* increases, the maximum *SWT* and maximum *U* tend to decrease gradually.

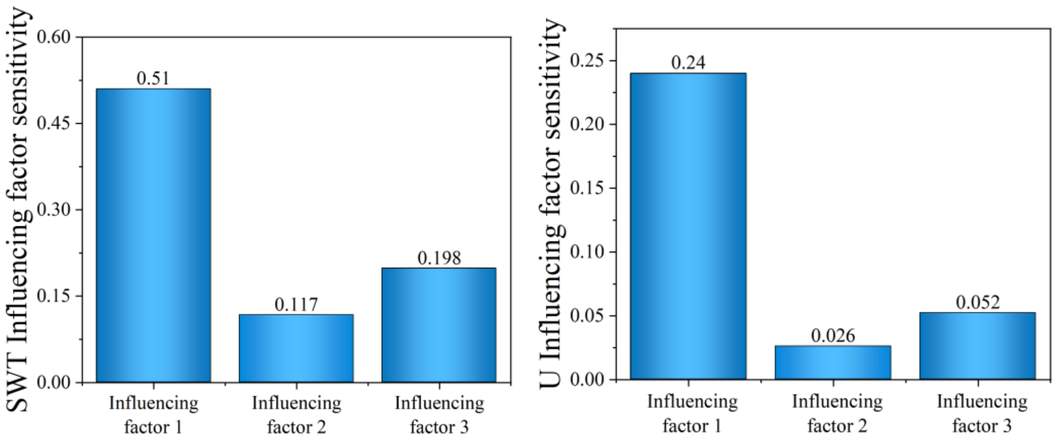

Figure 5: Sensitivity based on range analysis

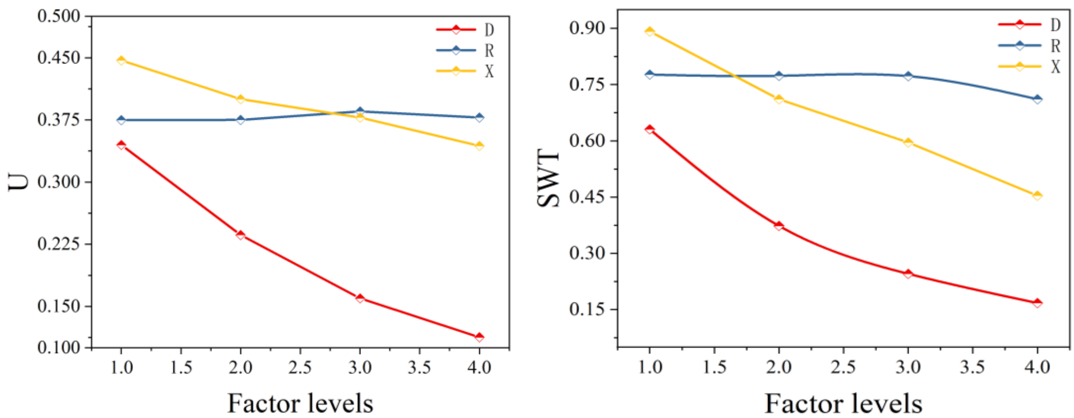

Figure 6: The changing trend of output under the influence of single factor

4.2 Multi-objective Optimization Approach

On the basis of the neural network model trained in 2.2, the relationship between each parameter combination and *SWT* and *U* can be obtained by establishing the PSO-BP neural network model, and all combinations within the parameter range can be predicted. Finally, the genetic algorithm is used to bring the pre-optimization parameter combination and the optimized optimal parameter combination into the neural network model respectively, and the corresponding results are obtained.

Considering the SWT and the U of the spring blade, the objective function is evaluated according to the artificial neural network corresponding to *SWT* and *U* trained in 2.2 above. The specific optimization process and size level are as follows. Different parameter combinations were brought into the neural network model to calculate the output values, and the optimal parameter combinations were found with the goal of minimizing the *SWT* and maximizing the *U*.

$$\mathrm{SWT}=\mathrm{net}_{\mathrm{SWT}}(D,R,X) \tag{5}$$

$$U=net_U(D,R,X) \tag{6}$$

$$D\in[0.3,0.55], R\in[0.7,2], X\in[3.6,4.5] \tag{7}$$

$\mathrm{net}_{\mathrm{SWT}}$ and $\mathrm{net}_{\mathrm{U}}$ are the neural network models trained with *SWT* and *U* as outputs, respectively. D is the thickness, R is the radius of the transition fillet, and X is the width.

Table 5: Parameter setting of NSGA- II

Parameter	Value
Crossover Fraction	0.8
Mutation Fraction	0.05
Population Size	200
Generations	100

The specific operating parameters of the NSGA-II. algorithm are shown in Table 5, and then the TOPSIS method is used to rank the Pareto frontier solutions to obtain the optimal solution.

4.3 Multi-objective Optimization Analysis

The Pareto optimal solution set of the NSGA-II. algorithm to solve the *SWT* and *U* is shown in Figure 7, and if the small *SWT* is blindly pursued without considering *U*, the work efficiency of the spring sheet will be seriously affected. Therefore, in the design process of spring sheets, both *SWT* and *U* factors should be considered. On the premise that the *U* is larger and can maintain normal work efficiency, the *SWT* value should be reduced as much as possible.

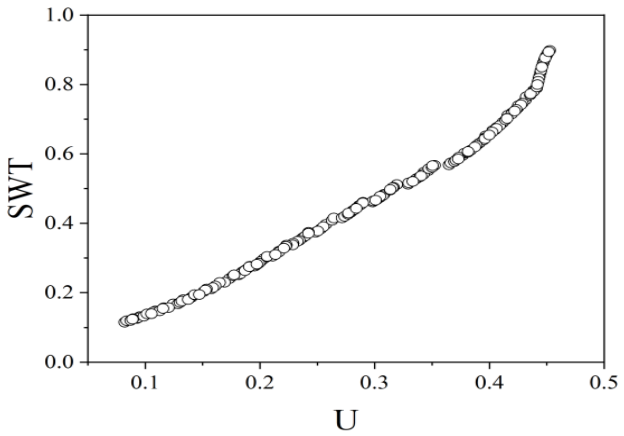

Figure 7: Optimization results of SWT and U

Table 6: Optimization result

	D	*R*	*X*	*SWT*	*U*
Raw value	0.35	1	3.6	0.498029	0.268158
Optimize the value	0.32	2	4.13	0.4438763	0.3043495
Verify the value	0.32	2	4.13	0.425982	0.305126

Table 6 shows the results before and after optimization. Comparing the data before and after optimization, it can be seen that the parameter combination obtained by the NSGA-II. algorithm is reduced by 10.9% and the displacement is increased by 13.5% compared with the parameter group *SWT*, and the thickness *D* is 0.32mm, the bifurcation width radius *R* is 0.2mm, and the bifurcation width *X* is 4.13mm. Subsequently, the finite element method was used to verify the optimized data, and the *SWT* error was 4%, the displacement error was 0.25%, and the errors were within the range of 5%. It can be seen that the results obtained by the genetic algorithm optimization are better than those in the orthogonal experimental group, which effectively reduces the *SWT* of the springs while ensuring the higher *U* of the springs and thus ensuring the work efficiency.

5. Conclusion

(1) This study is based on a finite element structural dataset and has trained a PSO-BP artificial neural network model capable of accurately predicting the SWT and displacement of spring leaves. And according to different data division, it is proved that it has a certain generalization ability. Therefore, the trained PSO-BP model is feasible as a surrogate model for predicting SWT damage parameters and displacements of spring blades.

(2) According to the results of parameter analysis, it can be seen that for the *SWT* and *U* of spring blades, thickness is a more significant factor than the radius and width of the circular line.

(3) Based on the optimization method and the combination of improved PSO-BP neural network and NSGA-II., the three design parameters of the spring blade were optimized, and the *SWT* and displacement of the spring blade were considered, and the results of the optimization method can minimize the damage parameters while meeting the requirements of work efficiency.

References

[1] Q. He, X. Wu, B. Gan, et al. Study on Characteristics and Application of Micro Air Pump [J]. Electronic technology, 2022, 51(4): 284-285.

[2] A.B. Beate, C.D. Patricia, H.S.K. Alexander, et al. Piezoelectric titanium based microfluidic pump and valves for implantable medical applications [J]. Sensors and Actuators: A. Physical, 2021, 323: 112649.

[3] L. He, H. Akebono, A. Sugeta, et al. Cumulative fatigue damage of stress below the fatigue limit in weldment steel under block loading [J]. Fatigue & Fracture of Engineering Materials & Structures, 2020, 43(7): 1419-1432.

[4] B.M. Naderi, M. Amiri, M.M. Khonsari. On the thermodynamic entropy of fatigue fracture [J]. Proceedings: Mathematical, Physical and Engineering Sciences, 2010, 466(2114): 423-438.

[5] S. Lin, W. Long, D. Tian, et al. A new fatigue damage accumulation model considering loading history and loading sequence based on damage equivalence [J]. International Journal of Damage Mechanics, 2018, 27(5): 707-728.

[6] Y. Xu, Z. Sun, Y. Zhang. The fretting fatigue experiments and finite element analysis of the friction type high-strength bolt joints [J]. Industrial Construction, 2017, 47(3): 175-181.

[7] Z. Xu, C. Liu, H. Feng. Fatigue-life prediction of hydraulic support’s front connecting rod based on finite-element analysis and RBF neural network [J]. Journal of Machine design, 2024, 41(1): 110-116.

[8] M. Zhang, D. Zeng, L. Lu, et al. Finite element modelling and experimental validation of bolt loosening due to thread wear under transverse cyclic loading [J]. Engineering Failure Analysis, 2019, 104: 341-353.

[9] S.O. Afolabi, B.I. Oladapo, C.O. Ijagbemi, et al. Design and finite element analysis of a fatigue life prediction for safe and economical machine shaft [J]. Journal of Materials Research and Technology, 2019, 8(1): 105-111.

[10] A. Ankit, C. Alok. Deep materials informatics: Applications of deep learning in materials science [J]. MRS Communications, 2019, 9(3): 779-792.

[11] S. Han, S. Khatir, M.W. Abdel. A deep learning approach to predict fretting fatigue crack initiation location [J]. Tribology International, 2023, 185: 108528.

[12] V.S. Srinivasan, M. Valsan, K. Bhanu Snakara Rao, et al. Low cycle fatigue and creep–fatigue interaction behavior of 316L(N) stainless steel and life prediction by artificial neural network approach [J]. International Journal of Fatigue, 2003, 25(12): 1327-1338.

[13] C. Peng, J. Chen, F. Feng. Optimization design for the stress-releaser of solid propellant gain based on genetic algorithm and neural network [J]. Journal of Solid Rocket Technology, 2014, 37(2): 198-203.

[14] S. Peng, Q. Zhang, H. Wang, et al. Coiled Tubing Fatigue Life Prediction Method Based on LMBP Algorithm of Neural Network [J]. Petroleum tubular goods & instruments, 2018, 4(6): 36-40.

[15] X. Zhang, J. Gong, F. Xuan. A deep learning based life prediction method for components under creep, fatigue and creep-fatigue conditions [J]. International Journal of Fatigue, 2021, 148: 106236.

[16] A.G.O. Brito, C.R.J.F. Silverio, A.L.M.C. Veloso, et al. A hybrid ANN-multiaxial fatigue nonlocal model to estimate fretting fatigue life for aeronautical Al alloys [J]. International Journal of Fatigue, 2022, 162: 107011.

[17] S. Xin. Multi-objective optimization design of of automobile leaf spring bracket based on genetic algorithm and BP neural network [J]. Journal of machine design, 2022, 39(12): 89-95.

[18] M.E. Fares, Y.G. Youssif, M.A. Hafiz. Structural and control optimization for maximum thermal buckling and minimum dynamic response of composite laminated plates [J]. International Journal of Solids and Structures, 2003, 41(3-4): 1005-1019.

[19] X. Peng, M. Wang, B. Yi, et al. Optimization design of stacking sequence and material distribution for variable thickness hybrid composite structure based on improved stacking sequence table [J]. Composite Structures, 2023, 307: 116614.

[20] Y. Song, J. Yang, Z. Xu, et al. Response Surface Optimization of Static Fatigue Characteristics of Joint bearings [J]. Machinery Design & Manufacture. 2022, (2): 229-232+236.

[21] M.H. Yas, A. Bayat, S. Kamarian, et al. Buckling analysis and design optimization of trapezoidal composite plates under hygrothermal environments [J]. Composite Structures, 2023, 315: 116935.